1   **Secondary Organic Aerosols from OH Oxidation of Cyclic Volatile Methyl Siloxanes as an Important**

2   **Si Source in the Atmosphere**

3   Chong Han[1,2], Hongxing Yang[1], Kun Li[2,3], Patrick Lee[2], John Liggio[2], Amy Leithead[2], Shao-Meng Li[4]*

4   [1]School of Metallurgy, Northeastern University, Shenyang, 110819, China

5   [2]Air Quality Research Division, Environment and Climate Change Canada, Toronto, Ontario M3H 5T4,

6   Canada

7   [3]Laboratory of Atmospheric Chemistry, Paul Scherrer Institute, Villigen 5232, Switzerland

8   [4]State Key Joint Laboratory of Environmental Simulation and Pollution Control, College of Environmental

9   Sciences and Engineering, Peking University, Beijing, China 100871

10   **Correspondence**: Shao-Meng Li (shaomeng.li@pku.edu.cn)

11

12   **Short summary:** We presented yields and compositions of Si-containing SOA generated from the reaction

13   of cVMS (D3-D6) with OH radicals. NO_x played negative roles on cVMS SOA formation, while ammonium

14   sulfate seeds enhanced D3-D5 SOA yields at short photochemical ages under high-NO_x conditions. The

15   aerosol mass spectra confirmed that the components of cVMS SOA significantly relied on OH exposure. A

16   global cVMS-derived SOA source strength was estimated to understand SOA formation potentials of cVMS.

17

18   **Abstract**

19   Cyclic volatile methyl siloxanes (cVMS) are active ingredients in widely used consumer products, which

20   can volatilize into the atmosphere, thus attracting much attention due to their potential environmental risks.

21   While in the atmosphere the cVMS undergo oxidation yielding both gaseous and particulate products. The

22   aerosol yields and compositions from the OH oxidation of four cVMS (D3-D6) were determined under low

23 and high-NO$_x$ conditions in an oxidation flow reactor. The aerosol yields progressively increased from D3

24 to D6, consistent with the volatilities and molecule weights of these cVMS. NO$_x$ can restrict the formation

25 of SOA, leading to lower SOA yields under high-NO$_x$ conditions than under low-NO$_x$ conditions, with a

26 yield decrease between 0.05-0.30 depending on the cVMS. Ammonium sulfate seeds exhibited minor

27 impacts on SOA yields under low-NO$_x$ conditions, but significantly increased the SOA yields in the oxidation

28 of D3-D5 at short photochemical ages under high-NO$_x$ conditions. The mass spectra of the SOA showed a

29 dependence of its chemical compositions on OH exposure. At high exposures, equivalent to photochemical

30 ages of >6 days in the atmosphere, D4-D6 SOA mainly consisted of C$_x$H$_y$ and C$_x$H$_y$O$_z$Si$_n$ under low-NO$_x$

31 conditions, whereas they primarily contained N$_m$O$_z$, C$_x$H$_y$, C$_x$H$_y$O$_1$, C$_x$H$_y$O$_{>1}$ and C$_x$H$_y$O$_z$Si$_n$ under high-NO$_x$

32 conditions. Using the yield data from the present study and reported cVMS annual production, a global

33 cVMS-derived SOA source strength is estimated to be 0.16 Tg yr^{-1}, distributed over major urban centers.

34

35 **1 Introduction**

36 Secondary organic aerosols (SOA), which contribute 50-85% to the mass of atmospheric organic aerosols

37 (OA) (Glasius and Goldstein, 2016), are mainly formed via the partitioning of low volatility products from

38 oxidation of volatile organic compounds (VOCs), semi- and intermediate volatile organic

39 compounds(S/IVOCs) (Riipinen et al., 2012). SOA has attracted significant attention due to their important

40 impacts on climate, ecosystems and human health (Berndt et al., 2016). Global budgets of SOA remain an

41 unresolved issue despite extensive research, largely due to uncertainties associated with aerosol yields and

42 the presence of unconsidered SOA precursors.

43 As one type of anthropogenic VOC and potential SOA precursors, cyclic volatile methyl siloxanes (cVMS)

44 are widely used in industrial applications and personal care products (Genualdi et al., 2011; Krogseth et al.,

45   2013a). cVMS have been classified as high-volume chemicals with an annual production of millions of tons

46   globally (Rücker and Kümmerer, 2015; Ahrens et al., 2014). Studies of cVMS in the environment have

47   focused on investigating health and environmental impacts particularly due to their potential persistence,

48   bioaccumulation and toxicity (Guo et al., 2019; Liu et al., 2018; Farasani and Darbre, 2017; Xu et al., 2019;

49   Kim et al., 2018; Coggon et al., 2018). As a result, the European Council has proposed a restriction on the

50   octamethylcyclotetrasiloxane (D4) and decamethylcyclopentasiloxane (D5) content in wash-off personal

51   care products to a limit of 0.1 mass% by 2020 (Eur-Lex, 2018). The legislative actions notwithstanding,

52   knowledge of environmental behavior of cVMS still needs to be further deepened as compared to their

53   applications and economic significance (Rücker and Kümmerer, 2015).

54   It has been estimated that approximately 90% of cVMS are emitted into the atmosphere due to their high

55   saturation vapor pressures (Allen et al., 1997). Gas-phase cVMS have been observed in both indoor and

56   outdoor air. Tang et al. (2015) reported that cVMS accounted for about one third of total VOC mass

57   concentration in a classroom. Outdoor air concentrations of cVMS have also been measured at different sites

58   worldwide (Li et al., 2020; Wang et al., 2018; Rauert et al., 2018), increasing from rural to urban sites and

59   consistent with increasing population density (Rücker and Kümmerer, 2015). For example, at a rural site in

60   Sweden, the concentration of hexamethylcyclotrisiloxane (D3), D4, D5 and dodecamethylcyclohexasiloxane

61   (D6) were 0.94, 3.5, 13 and 1 ng/m^3, respectively (Kierkegaard and Mclachlan, 2013), while they were 18,

62   55, 172 and 14 ng/m^3 in urban areas of Toronto in Canada, respectively (Genualdi et al., 2011; Rauert et al.,

63   2018). cVMS have also been detected in the remote Arctic atmosphere, confirming their long-range transport

64   (Genualdi et al., 2011; Krogseth et al., 2013b). Atmospheric half-lives of cVMS are on the order of 30, 15,

65   10 and 6 days for D3-D6, respectively, which allow cVMS to exhibit a hemispherical distribution in the

66   atmosphere (Canada, 2008; Xiao et al., 2015). These lifetimes are driven mostly by reactions with the OH

67   radicals (Xiao et al., 2015; Wang et al., 2013), which generate silanols and dimeric products that can be

68   partitioned to condensed phases (Coggon et al., 2018; Sommerlade, 1993; Wu and Johnston, 2016). The loss

69   of cVMS in the atmosphere is slight through O_3 and NO_3 due to their small reaction rates, and by Cl atoms

70   on account of its low concentration except for the spatial and temporal overlaps of cVMS emissions and Cl

71   sources (Atkinson, 1991; Alton and Browne, 2020).

72   It has been demonstrated that elemental Si is a frequent constituent of nanoparticles in rural and urban

73   areas (Phares et al., 2003; Rhoads, 2003; Bein, 2005; Bzdek et al., 2014) and in remote regions (Li and

74   Winchester, 1990; Li and Winchester, 1993). These Si-containing nanoparticles have previously been

75   attributed to ore smelting processes, but recent studies have shown that Si-containing species are one of the

76   main components in cVMS SOA, suggesting that the oxidation of cVMS may be an important source of Si

77   in atmospheric aerosols (Wu and Johnston, 2016, 2017). In a modeling study, the oxidation products of

78   cVMS (D4, D5 and D6) were considered to quantify the maximum potential for aerosol formation through

79   reactions with the OH radicals (Janechek et al., 2017). Chandramouli and Kamens (2001) demonstrated the

80   gas-particle partitioning of silanols from D5 oxidation by the OH radicals. Wu and Johnston (2016, 2017)

81   analyzed the chemical composition of secondary aerosols from OH oxidation of D4 and D5, showing a large

82   number of monomeric and dimeric products. Janechek et al. (2017, 2019) reported physical properties of

83   SOA generated by OH oxidation of D5, including hygroscopicity, cloud seeding potential and volatility.

84   Charan et al. (2022) measured SOA yields of D5 using chambers and flow tube reactors, emphasizing the

85   importance of the relevant OH concentrations and exposures when extrapolating these laboratory results or

86   comparing with other studies. These studies mainly focused on D5 and occasionally D4 but rarely others. To

87   better understand the SOA-forming potentials of typical cVMS in the atmosphere, accurate yields and

88   molecular compositions of SOA from the oxidation of cVMS under various atmospheric conditions are

89   needed.

90   In this work, the formation of SOA from the oxidation of four cVMS (D3-D6) by OH radical was

91   investigated in an oxidation flow reactor (OFR). Under various combinations of NO_x and ammonium sulfate

92   seed concentrations, the yields and compositions of SOA formed from the oxidation were measured using a

93   suite of instruments including a scanning mobility particle sizer (SMPS), a proton transfer reaction time of

94   flight mass spectrometer (PTR-ToF-MS) and an aerosol mass spectrometer (AMS). Based on these SOA

95   yields, the contribution of cVMS to SOA in the global atmosphere was estimated using reported cVMS

96   concentrations. The results obtained here can largely improve our understanding of the contribution and

97   composition of SOA from cVMS.

98   **2 Experiments and methods**

99   **2.1 Photo-oxidation experiments**

100   The reactions of cVMS with OH radicals were controlled at a constant temperature (21±1˚C) and relative

101   humidity (35%±2%) in a custom-made oxidation flow reactor (the Environment and Climate Change Canada

102   oxidation flow reactor, ECCC-OFR), which is shown in Fig. S1 of the Supplement and has been described

103   in detail previously (Li et al., 2019a). Briefly, the ECCC-OFR is a fused quartz cylinder (length: 50.8 cm,

104   inner diameter: 20.3 cm) equipped with a conical inlet and 7 outlets. Wall losses of particles and gases in the

105   ECCC-OFR have been shown to be lower than in other OFRs (Huang et al., 2017; Lambe et al., 2011;

106   Simonen et al., 2017; Li et al., 2019a). The length and full angle of cone inlet are 35.6 cm and 30°,

107   respectively, designed to minimize the formation of jetting and recirculation in the OFR. The outlet at the

108   reactor center is a stainless-steel sampling port (inner diameter: 0.18 in) extending 12.7 cm long into the

109   ECCC-OFR. This sampling inlet reduces the impact of potential turbulent eddies caused by the back end of

110   the reactor. The remaining 6 outlets around the perimeter are designed to allow side flows to pass through

111   the OFR as a sheath flow, indirectly reducing wall losses of gases and particles inside the OFR upon sampling.

112   Ozone-free mercury UV lamps for generating OH radicals are housed in small quartz tubes around and in

113   parallel to the quartz reaction cylinder, and a large flow of air through each of these smaller quartz tubes is

114   used to remove the heat produced by the lamps. The relative humidity was adjusted by controlling the ratio

115   of dry air to wet air into the reactor, and was measured using a humidity sensor (Vaisala) at one of the sheath

116   flow outlets (side flows) of the reactor. The volume of the entire ECCC-OFR is about 16 L and the total flow

117   rate is 8 L min^{-1}, leading to a residence time of 2 min in the OFR.

118   OH radicals were produced through the reaction of water vapor with O(^{1}D) formed from O_3 photolysis at

119   254 nm. The OH concentration in the ECCC-OFR was regulated by controlling the input voltage and the

120   number of UV lamps. Methanol vapor, introduced into the ECCC-OFR through a bubbler containing

121   methanol solution, was used to determine the OH exposure (i.e., photochemical age) by tracking its decay

122   in the reactor from the reaction with the OH. The decay, or fractional loss, of gas-phase methanol,

123   [MeOH]/[MeOH]$_0$ was measured with the PTR-ToF-MS, and was used to calculate the OH concentration

124   via Equation 1,

125                                    $$[OH] = -\frac{1}{k_{MeOH}} \ln \frac{[MeOH]}{[MeOH]_0}$$ (1)

126   where k_{MeOH} is the second-order rate constant of methanol reaction with OH at 298 K (9.4×10^{-13} cm^3

127   molecule^{-1} s^{-1}). It was noted that the OH exposure measurement was offline, because methanol can affect the

128   OH reactivity with cVMS. Under low and high-NO$_x$ conditions described below, the OH exposure varied in

129   the range of 5.5×10^{10}-1.8×10^{12} and 8.2×10^{10}-1.1×10^{12} molecules cm^{-3} s, respectively. They correspond

130   to 0.4-14.2 and 0.6-8.5 equivalent days (photochemical age), respectively, assuming that an average OH

131   concentration in air is 1.5×10^6 molecules cm^{-3} (Mao et al., 2009).

132   Pure D3-D6 cVMS compounds (solid D3 and liquid D4, D5 and D6) were placed in a glass U-type tube

133   and maintained at the room temperature. Vapors from these compounds (Table S1 of the Supplement) were

134   separately introduced into the ECCC-OFR by a small flow of zero air (1-18 mL min^{-1}) passing over the

135   headspace of the U-tube containing the pure compounds. The concentrations of D3-D6 in the ECCC-OFR

136   ranged from 18 to 46 ppb (Table S2), depending on their volatilities. To study the influence of existing

137   particles on the SOA formation, ammonium sulfate (AS) seed particles were produced using an atomizer,

138   dried by a diffusion dryer and neutralized by a neutralizer and injected into the reactor without size selection.

139   The mass concentration of AS seed particles was approximately 30 μg m^{-3} for all experiments.

140   N$_2$O was used as a source of NO to achieve high-NO$_x$ conditions (Lambe et al., 2017). NO$_x$ conditions

141   were defined by the fate of peroxy radicals (RO$_2$), which was described by the reaction rate ratio (R_{NO}) of

142   RO$_2$ + NO and RO$_2$ + HO$_2$ (Peng et al., 2017). The R_{NO} ratio increases with increasing OH exposures at a

143   constant concentration of N$_2$O (Li et al., 2019b). To achieve a constant branching ratio during the high-NO$_x$

144   experiments, the initial N$_2$O concentration in the OFR was varied (1.6%-8.0%) to maintain an R_{NO} value of

145   20 (Li et al., 2019b), as calculated using a model (OFR Exposures Estimator v3.1) (Peng et al., 2017). A

146   ratio of R_{NO}=20 indicates that 95% of RO$_2$ reacts with NO, ensuring the dominance of RO$_2$ + NO, which

147   represents conditions that are relevant for urban atmosphere (Peng et al., 2019). The role of RO$_2$ + RO$_2$ here

148   should be minor or negligible due to the low concentration of SOA precursors (cVMS, 18-46 ppb) (Lambe

149   et al., 2017; Peng et al., 2019; Li et al., 2019b). Peng et al. (2019) have reported that in the experiments

150   utilizing the injection of N$_2$O to achieve high-NO$_x$ conditions, the relative importance of RO$_2$ + OH was

151   generally negatively correlated with N$_2$O due to the suppressing effect of NO$_x$ on OH radicals and the

152   increasing role of RO$_2$ + NO. Under low-NO$_x$ conditions, N$_2$O was not introduced into the OFR, where the

153   RO$_2$ radicals dominantly interacted with HO$_2$ radicals, representing atmospheric scenarios with few NO$_x$

154   sources.

2.2 Characterization and analysis

The concentrations of cVMS in the OFR were measured online with PTR-ToF-MS (Ionicon Analytik GmbH) (Liggio et al., 2016). The number and mass size distribution of aerosols was monitored using a scanning mobility particle sizer (SMPS, TSI). The mass spectra and elemental composition of aerosols was determined with a high-resolution time-of-flight aerosol mass spectrometer (HR-ToF-AMS, Aerodyne) and analyzed with the AMS analysis software Squirrel (version 1.62G) and Pika (version 1.22G).

SOA mass yields (Y) were calculated via Equation 2,

$$Y = \frac{\Delta C_{\text{SOA}}}{\Delta C_{\text{cVMS}}} \qquad (2)$$

where ΔC_{SOA} and ΔC_{cVMS} are the mass concentrations of SOA formed and cVMS lost, respectively. The mass concentration of SOA was determined by multiplying the effective aerosol density by the integrated SOA volume concentration from the SMPS, subtracting the AS seed volume for experiments with AS seeds. The effective aerosol density (ρ) was calculated for unseeded experiments through the following Equation 3 (Lambe et al., 2015),

$$\rho = \frac{D_{va}}{D_m} \qquad (3)$$

where D_{va} is the vacuum aerodynamic diameter obtained from the HR-ToF-AMS, and D_m is the electric mobility diameter measured by the SMPS. The ρ varied in the range of 1.6-1.8 depending on the cVMS. The same ρ value was also used in the seeded experiments. It should be pointed out that the background values in Table S3 have been subtracted when calculating the cVMS SOA yields.

3 Results and discussion

3.1 SOA yields

Taking the D5 SOA under low-NO$_x$ and unseeded conditions as an example, the number and mass size distributions of aerosols were shown in Fig. S2, which indicated that small particles dominated in the number,

8

177   while large ones were prominent in mass. Compared to the size distributions of D5 SOA in low-NO$_x$

178   experiments (Fig. S2a), the mode diameter of SOA increased for both number and mass size distribution

179   under high-NO$_x$ conditions (Fig. S2b), which suggests that larger particles are dominant in D5 SOA

180   generated in high-NO$_x$ experiments. The mass concentrations and time series of SOA measured by SMPS

181   and AMS were shown in Table S4 and Fig. S3, respectively, which reflected a step-by-step pattern with

182   increasing OH exposures.

183   Figure 1 shows the SOA yields from the photooxidation of the D3-D6 cVMS under low and high-NO$_x$

184   conditions as a function of photochemical age (PA), i.e., time-integrated OH exposure, with and without AS

185   seed particles. SOA yields have been widely used to estimate the potential of precursors to produce aerosol

186   mass (Mcfiggans et al., 2019; Li et al., 2019a; Bruns et al., 2015; Lambe et al., 2015). As shown in Fig. 1,

187   the cVMS SOA yields exhibited an overall increasing trend with PA, expressed in equivalent photochemical

188   days, which agreed with the trend of D5 SOA yields reported by Janechek et al. (2019). Under low-NO$_x$

189   conditions (Fig. 1a), SOA yields exhibited a slow growth, reaching a plateau after 10 equivalent days. This

190   may be due to increased gas-phase fragmentation of cVMS to generate some higher volatility products,

191   leading to a small increasing amplitude of partition ratio of species into SOA at longer photochemical ages.
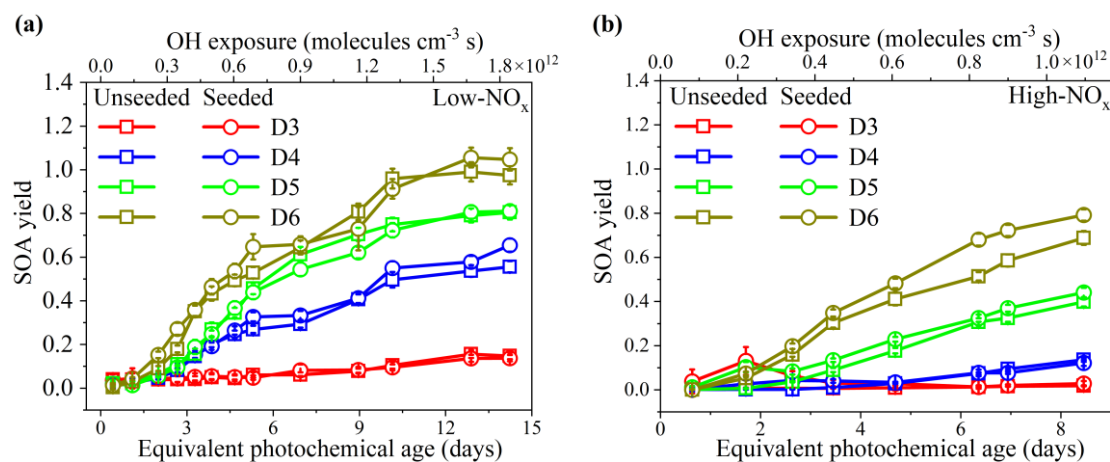
192

193   Figure 1. SOA yields from unseeded and seeded (30 μg m^{-3}) photooxidation of cVMS by OH radicals. **(a)**

194   low-NO$_x$ experiments; **(b)** high-NO$_x$ experiments.

195   For the unseeded and low-NO_x experiments in Fig. 1a, SOA yields of four cVMS exhibited significant

196   differences in values over the same number of equivalent days. The SOA yields successively increased from

197   D3 to D6, consistent with the volatilities and molecular masses of the cVMS as well as their reaction rate

198   constants with the OH radical (Alton and Browne, 2020; Kim and Xu, 2017; Safron et al., 2015). The

199   maximum SOA yields of D3-D6 were (0.16±0.02), (0.56±0.03), (0.80±0.03) and (0.99±0.04), respectively,

200   occurring after a PA of 12 equivalent days. It has been reported that D5 SOA yields varied in the range of 0-

201   1.1 (Janechek et al., 2019; Wu and Johnston, 2017; Charan et al., 2022). Under a low OH exposure ($\sim10^{10}$-

202   10^{11} molecules cm^{-3} s), the D5 SOA yield (0.01-0.11) obtained here was similar to that (chamber, 0-0.057;

203   flow tube, 0.018-0.06) measured by Charan et al. (2022). However, under a high OH exposure of $\sim10^{11}$-10^{12}

204   molecules cm^{-3} s, the D5 SOA yield of 0.46-0.70 was higher than 0.22 and 0.14-0.35 (flow tube) reported

205   by Janechek et al. (2019) and Charan et al. (2022), respectively, which may be attributed to differences in

206   experimental conditions, such as differences in reactors, wall losses, SOA measurement methods,

207   determination of OH concentrations, and initial D5 concentrations (Table S5) (Janechek et al., 2019; Charan

208   et al., 2022). Although the amount of cVMS lost was variable, cVMS SOA yields positively depended on

209   SOA mass concentrations (Fig. S4), and this trend was observed in previous D5 SOA experiments with OH

210   oxidation (Wu and Johnston, 2017).

211   As shown in Fig. 1b, the order of SOA yields from the four cVMS under high-NO_x conditions was the

212   same as that under low-NO_x conditions. However, the SOA yields under high-NO_x conditions were generally

213   smaller than the corresponding yields at similar OH exposures under low-NO_x conditions, with a decrease

214   of 0.05-0.30 depending on the cVMS. Such a reduction suggests that NO_x can restrict the formation of cVMS

215   SOA. NO_x has been shown to reduce SOA yields for some anthropogenic alkanes (Li et al., 2019b), aromatics

216   (Ng et al., 2007a; Chan et al., 2009; Zhou et al., 2019), monoterpenes (Zhao et al., 2018) and other terpenes

217   (Ng et al., 2007b), attributable to the formation of higher volatility products (e.g., organic nitrates) generated

218   by $RO_2 + NO$ compared to $RO_2 + HO_2$ (Presto et al., 2005; Li et al., 2019b), which is also likely the case

219   here. The higher volatility products favor partitioning in the gas phase, thus reducing the potential for

220   forming SOA (Zhou et al., 2019). Moreover, high NO_x levels can suppress the formation of products for

221   nucleation, thereby reducing aerosol surface as a condensational sink and increasing the wall loss of

222   condensable species in an OFR under high-NO_x conditions (Zhao et al., 2018; Sarrafzadeh et al., 2016; Wildt

223   et al., 2014). Figure S5 indicates that the difference between SOA yields with and without NO_x decreased

224   with increasing silicon atoms within individual cVMS, indicating a less restricting effect of NO_x on the SOA

225   formation for larger cVMS. This means that high NO_x levels play a lessor role in the SOA yields of lower

226   volatility precursors.

227   SOA yields in the AS-seeded experiments under low and high-NO_x conditions are also shown in Figs. 1

228   and S5, indicating minimal impacts of the AS seed particles on SOA yields. A yield enhancement ratio

229   ($R_E = Y_{seeded}/Y_{unseeded}$, Fig. S6) was used to show the seed impacts more clearly. Under low-NO_x conditions,

230   the R_E values for all cVMS were close to 1.0 (Fig. S6a), suggesting negligible impact of AS seed particles

231   on SOA yields; however, under high-NO_x conditions, R_E was much larger (17.81, 13.18 and 15.51 for D3-

232   D5, respectively) at short PA but gradually decreased to 1.0 with increasing PA for D3-D5, while it was

233   always close to 1.0 for D6 regardless of PA (Fig. S6b). R_E values greater than 1.0 suggest that AS seed

234   particles played an enhancement role in the cVMS SOA formation, as similarly reported in SOA formation

235   from hydrocarbons (Sarrafzadeh et al., 2016; Lamkaddam et al., 2017; Li et al., 2019b). Under low-NO_x

236   conditions, the general lack of impact on cVMS SOA yields by the AS seed particles suggests that

237   condensation was not the main process driving SOA formation in cVMS oxidation. For the few cases of high

238   NO_x level at low PA, where R_E was >1 for D3-D5, it is possible that their early generations of oxidation

239   products were more volatile than successive generations of products and hence more prone to condensation

240   enhanced by AS seeds. As PA increased, further reactions of these early generation oxidation products with

241   OH radicals resulted in further generation products that were likely less volatile, thereby weakening the

242   enhancing role of AS seeds at high OH exposure. Such effect was less pronounced for D6, likely because its

243   oxidation products at different PA had similar volatilities. Figure S6b shows that the effect of AS seed

244   particles on SOA yields negatively correlated with the number of silicon atoms in the cVMS. Lower volatility

245   precursors (D5 and D6) may form lower volatile products, resulting in SOA yields less sensitive to the pre-

246   existing seeds. In fact, the oxidation products of D5 have been shown to be nearly non-volatile (Janechek et

247   al., 2019; Wu and Johnston, 2017).

248   **3.2 Aerosol compositions**

249   **3.2.1 Compositions of SOA under low-NO_x conditions.**

250   Figures 2 and S7 show the normalized HR-ToF-AMS mass spectra of cVMS SOA from unseeded

251   experiments under low-NO_x conditions at OH exposures of 9.0×10^{11} molecules cm^{-3} s. The mass spectral

252   signals can be identified as fragments with a formula of $C_xH_yO_zSi_n$. For D3 SOA, the most prominent peaks

253   were at m/z 44 and 29, dominated by CO_2^+ and CHO^+, which were tracers for organic acids (Ng et al., 2010),

254   alcohols and aldehydes (Lee et al., 2012), respectively. They may result from the oxidation of the methyl

255   groups in D3 by OH radicals. For the mass spectra of D4-D6 SOA, the two highest peaks at m/z 14 and 15

256   were CH_2^+ and CH_3^+, respectively. In addition, there were several dominant $C_xH_yO_zSi_n$ peaks, which were

257   fragments of silicon-containing products. For the $C_xH_yO_zSi_n$ group in D4 SOA, there were four typical peaks

258   at m/z 255, 257, 271 and 273, with formulae of $C_4H_{11}O_7Si_3^+$, $C_3H_9O_8Si_3^+$, $C_3H_7O_9Si_3^+$ and $C_3H_9O_9Si_3^+$,

259   respectively. The $C_xH_yO_zSi_n$ fragment group containing Si of D5 SOA had three dominant peaks at m/z 327,

260   329 and 331, corresponding to $C_{12}H_{11}O_2Si_5^+$, $C_9H_9O_8Si_3^+$ and $C_5H_{15}O_9Si_4^+$, respectively. For the $C_xH_yO_zSi_n$

261   group containing Si in D6 SOA, there were five main peaks at m/z 73 (C_3H_9Si), 387 ($C_8H_{23}O_8Si_5^+$), 389

262   ($C_8H_9O_9Si_5^+$), 401 ($C_9H_{21}O_{10}Si_4^+$) and 403 ($C_7H_{15}O_{12}Si_4^+$).
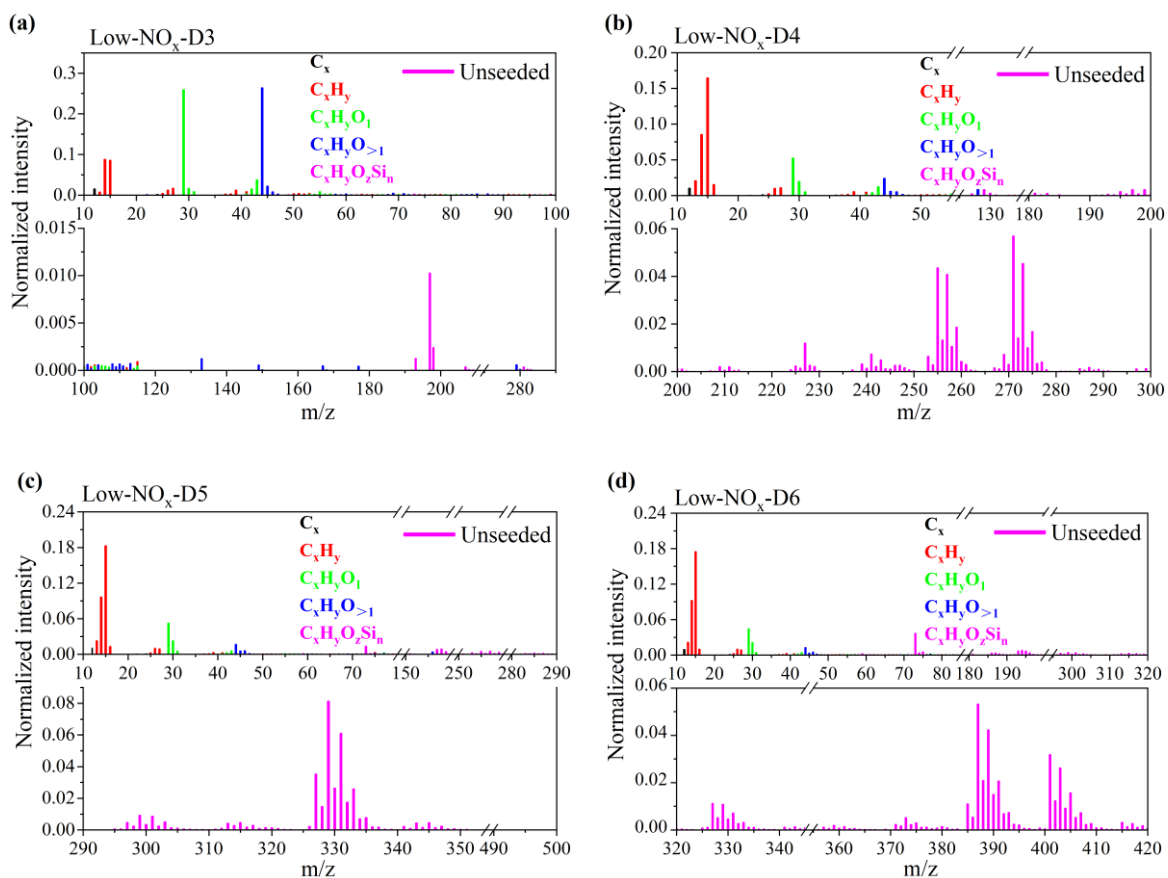
263

264

265   Figure 2. HR-ToF-AMS mass spectra of cVMS SOA at OH exposure of 9.0×10^{11} molecules cm^{-3} s under

266   low-NO$_x$ conditions in unseeded experiments. **a-d** represent the mass spectra of D3-D6 SOA, respectively.

267

268   Figure 3 shows the evolution of different groups of ions in the HR-ToF-AMS spectra of the cVMS SOA

269   as a function of PA in equivalent days. For D3-D6 under unseeded conditions, $C_xH_yO_1$ and $C_xH_yO_{>1}$ ions

270   significantly decreased within 0-4 equivalent days of PA, but remained essentially unchanged when PA

271   increased to 7-15 equivalent days. The C_xH_y ion increased to its peak value at about 9 equivalent days of PA

272   for D3 and 2-3 equivalent days of PA for D4-D6, and then gradually decreased with further PA increases.

273   The $C_xH_yO_zSi_n$ group of ions maintained an increasing trend until 9-10 days of PA, thereafter it decreased

274   slightly for D4-D6 SOA. The weighted values of the atomic number ratios Si/C (n/x) and Si/O (n/z) for the

275   $C_xH_yO_zSi_n$ groups in D5 and D6 SOA at different PA are plotted in Fig. S8, which can be used to indicate

276   the changes in the Si element of SOA. The Si/C ratio at initial SOA formation stage was close to that (0.50)

277   in D5 and D6 molecules, and then increased continuously with increasing PA. The Si/O ratio kept increasing

278   from 0.53 to 1.15 for D5 SOA and from 0.72 to 1.32 for D6 SOA, but varying around 1.0 that was the Si/O

279   ratio in D5 and D6. While it is difficult to separate the effect of fragmentation due to the AMS ionization

280   process, the relative changes of group intensities and the evolution of Si/C and Si/O in $C_xH_yO_zSi_n$ over

281   different PA may be attributed to the evolution of cVMS when oxidized by the OH radicals. The initial step

282   of OH radicals oxidation can be considered as OH abstracting a H atom from the methyl groups on the -Si-

283   O- ring of the cVMS to form Si-containing radicals, which may generate OH and CH_2OH substitution

284   products, such as silanol and silyl methanol (Wu and Johnston, 2016; Alton and Browne, 2020). Such Si-

285   containing products may partition into SOA and result in an appearance of $C_xH_yO_zSi_n$ ions in the AMS mass

286   spectra, thereby decreasing the initial ratio of Si/O (D5: 0.53; D6: 0.72). Notably, one previous study reported

287   that one of oxidation products of D5, 1- hydroxynonamethylcyclopentasiloxane (D_4TOH), has been detected

288   in ambient particulate matter (Milani et al., 2021). As the reaction progresses, the Si-O bonds may be cleaved

289   from OH radical attack, which may reduce the number of O atoms, leading to an increase of Si/O with PA.

290   The continued breaking of Si-O bonds would lead to fragmentation and more volatile products, which caused

291   lower SOA yield and $C_xH_yO_zSi_n$ fraction at longer PA (Figs. 1 and 3).

292

293
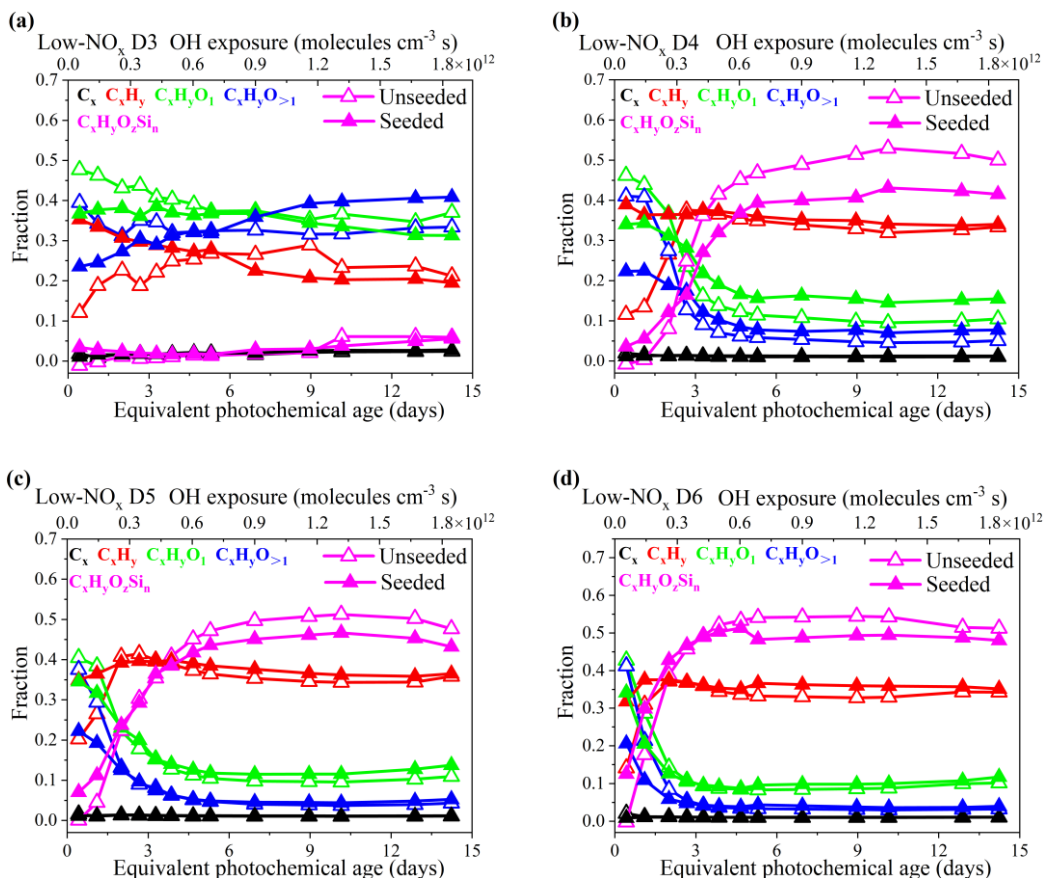
Figure 3. Fraction of C_x, C_xH_y, $C_xH_yO_1$, $C_xH_yO_{>1}$ and $C_xH_yO_zSi_n$ ion groups for SOA derived from the

oxidation of cVMS (**a-d**) by OH radicals at different photochemical ages under low-NO_x conditions.

Empty and solid triangles represent experimental data under unseeded and seeded conditions, respectively.

As shown in Fig. 3, the presence of seeds led to some changes in the evolution trends of ion groups in the

AMS spectra. For instance, the initial fraction of C_xH_y in seeded experiments was larger than that in unseeded

experiments, which may be related to the volatility of species containing C_xH_y that may be more easily

deposited in the presence of seeds, whereas $C_xH_yO_1$ and $C_xH_yO_{>1}$ exhibited opposite changes. The presence

of seeds led to larger initial and smaller steady-state $C_xH_yO_zSi_n$ fractions than those in unseeded experiments.

Regardless of the presence of seeds, C_xH_y, $C_xH_yO_1$ and $C_xH_yO_{>1}$ mainly contributed to the composition of

all cVMS SOA at initial OH radicals oxidation, but D4-D6 SOA primarily consisted of C_xH_y and $C_xH_yO_zSi_n$

15

305   after 6 equivalent days.

306   **3.2.2 Compositions of SOA under high-NO$_x$ conditions.**

307   Figure S9 shows the HR-ToF-AMS mass spectra of cVMS SOA from unseeded experiments under high-

308   NO$_x$ conditions at OH exposures of 9.0×10^{11} molecules cm^{-3} s (~6.9 d). Compared to that under low-NO$_x$

309   conditions (Figs. 2 and S7), there was one additional N-containing group (N$_m$O$_z$) in the SOA mass spectra

310   under high-NO$_x$ conditions, which accounted for 16%-31%. For the mass spectra of D3-D6 SOA originating

311   from unseeded experiments under high-NO$_x$ conditions in Fig. S9, the dominating peaks of the N$_m$O$_z$ family

312   were m/z 30 (NO$^+$) and m/z 46 (NO$_2^+$). The common main peaks were located at m/z 30 (NO$^+$) for cVMS

313   SOA, m/z 44 (CO$_2^+$) for D3-D4 SOA, and m/z 46 (NO$_2^+$) for D4-D6 SOA. In addition, there were other

314   primary peaks at m/z 29 (CHO$^+$) for D4 SOA, while m/z 15 (CH$_3^+$) and m/z 28 (CO$^+$) for D5-D6 SOA. The

315   m/z 28 (CO$^+$), similar with m/z 44 (CO$_2^+$), is considered as a tracer for organic acids (Ng et al., 2010). In the

316   mass spectra for D3-D6 SOA under high-NO$_x$ conditions, the presence of NO$^+$ (m/z 30) and NO$_2^+$ (m/z 46)

317   illustrated the formation of nitrates in SOA (Ng et al., 2007b).

318   For the C$_x$H$_y$O$_z$Si$_n$ group in the D4 SOA mass spectrum under high-NO$_x$ conditions, the dominating peaks

319   and their formulas were same as those under low-NO$_x$ conditions. For the C$_x$H$_y$O$_z$Si$_n$ group in D5 SOA, in

320   addition to two typical peaks at m/z 327 and 329 in the low-NO$_x$ experiments, there was another prominent

321   peak at m/z 328, with a formula C$_8$H$_{12}$O$_5$Si$_5$. The C$_x$H$_y$O$_z$Si$_n$ group in D6 SOA had three typical peaks at m/z

322   73 (C$_3$H$_9$Si), m/z 387 (C$_8$H$_{23}$O$_8$Si$_5^+$) and m/z 401 (C$_9$H$_{21}$O$_{10}$Si$_4^+$). For the C$_x$H$_y$O$_z$Si$_n$ groups in cVMS SOA,

323   there was little difference in the x, y, z and n value assignment of C$_x$H$_y$O$_z$Si$_n$ peaks in SOA generated under

324   low-NO$_x$ and high-NO$_x$ conditions, suggesting the formation of similar Si-containing oxidation products.

325   For cVMS SOA under high-NO$_x$ conditions, the evolution of family groups as a function of OH exposure

326   was summarized in Fig. S10. The dominated composition at initial stage was C$_x$H$_y$O$_{>1}$ groups for D3-D6

16

327   SOA. At equivalent days larger than 6, D3 SOA primarily consisted of $C_xH_yO_{>1}$, N_mO_z and $C_xH_yO_1$ groups,

328   while D4-D6 SOA was mainly composed of $C_xH_yO_zSi_n$, N_mO_z, $C_xH_yO_1$, C_xH_y and $C_xH_yO_{>1}$ groups. Figure

329   S10 also shows influences of seeds on the evolution of family groups under high-NO_x conditions. It was

330   observed that all groups in D3-D6 SOA displayed similar change trends regardless of the existence of seeds.

331   As shown in Fig. S11, the trend of the weighted values of the atomic ratio Si/O in the $C_xH_yO_zSi_n$ groups at

332   different photochemical ages under high-NO_x conditions was similar to that in low-NO_x experiments.

333   However, the Si/C ratios remained almost unchanged, and were close to the initial value (0.5) in cVMS. This

334   may be attributed to possible suppression of cleavage of methyl groups from the -Si-O- ring of the cVMS

335   under high-NO_x conditions.

336   **4 Conclusions and implications**

337   The yields and compositions of SOA generated from the photooxidation of four cVMS (D3-D6) with OH

338   radicals were investigated using an oxidation flow reactor. cVMS SOA yields exhibited an overall increasing

339   trend with PA, and their values gradually increased with cVMS from D3 to D6. SOA formations depended

340   on NO_x, as shown by smaller SOA yields under high-NO_x conditions. Ammonium sulfate seeds significantly

341   enhanced SOA yields of D3-D5 at short PA under high-NO_x conditions. The SOA mass spectra showed that

342   Si-containing species were one of main chemical compositions at PA of >6 days.

343   To evaluate the potential contributions of cVMS to SOA formation in the atmosphere, global SOA

344   concentrations produced from cVMS were estimated according to the cVMS SOA yields measured in this

345   work and using the cVMS concentrations reported from multiple studies, which were listed in Table S6.

346   Here, the high-NO_x SOA yields under the seeded conditions at 8.5 equivalent days (D3: 0.028; D4: 0.122;

347   D5: 0.441; D6: 0.792) are employed in the calculation of cVMS SOA concentrations at urban sites, while

348   the low-NO_x SOA yields under the unseeded conditions at 14.2 equivalent days (D3: 0.148; D4: 0.556; D5:

349   0.805; D6: 0.975) are used to estimate cVMS SOA at background and polar sites. The selected equivalent

350   days were within the atmospheric half-lives (6-30 days) of cVMS. Figure 4 shows the global concentration

351   distribution of SOA from four cVMS (D3-D6) at 36 sites worldwide estimated by the Equation 4,

$$C_{\text{cVMS-SOA}}=C_{\text{cVMS}}\times\frac{\Delta C_{\text{cVMS}}}{C_{\text{in-cVMS}}}\times Y \qquad (4)$$

353   where C_{cVMS} and $C_{\text{cVMS-SOA}}$ are the mass concentration of cVMS reported from literatures and cVMS SOA

354   estimated in global sites, respectively; $C_{\text{in-cVMS}}$ and ΔC_{cVMS} are the mass concentration of initial and lost

355   cVMS at the selected equivalent days during the experiments of this work, respectively (Table S7); Y is the

356   cVMS SOA mass yields mentioned above. It was noted that the estimations from the Equation 4 were based

357   on assumptions that the lost cVMS ratio is not affected by the cVMS concentration and the background

358    $C_{\text{cVMS-SOA}}$ is zero. Although there may be some uncertainties in extrapolating our results to the real

359   atmosphere, such as larger cVMS concentrations and SOA yields, our extrapolations may provide an upper

360   limit for evaluating cVMS SOA. Table S6 summarizes the details regarding sites and concentrations of

361   cVMS SOA. The derived concentrations of cVMS SOA varies significantly among urban, background and

362   polar sites. The total cVMS SOA concentrations in urban areas are the highest, up to 1324 ng/m^3. They are

363   18.9-428 and 13.8-138.8 ng/m^3 for background and Arctic sites, respectively. cVMS SOA concentrations in

364   urban regions of Asia (sites 29-36) and Europe (sites 26-28) are generally larger than that of North America

365   (sites 20-25). In China, the total cVMS SOA concentrations in urban sites range from 15.5 to 1324 ng/m^3.

366   The main precursors of cVMS SOA are different among Chinese cities. For three cities along the southeast

367   coast of China (Guangzhou, Macau and Foshan), the dominant precursors of cVMS SOA are D3 and D4,

368   which are related to industrial emissions of these two siloxanes in this region (Wang et al., 2001). For Dalian

369   in China, mainly D5 and D6 contribute to cVMS SOA, which have the highest concentrations among all

370   sites. This can be attributed to the industrial production of D5 and D6 and the use of personal care products

371   in Dalian (Li et al., 2020). In the other Chinese urban areas with reported cVMS concentrations (Lhasa,

372   Golmud, Kunming and Yantai), the total cVMS SOA concentrations are considerably smaller than those in

373   the urban areas above, with D5 acting as the main precursor, which may be ascribed to the relatively low

374   population densities in these cities (Wang et al., 2018).
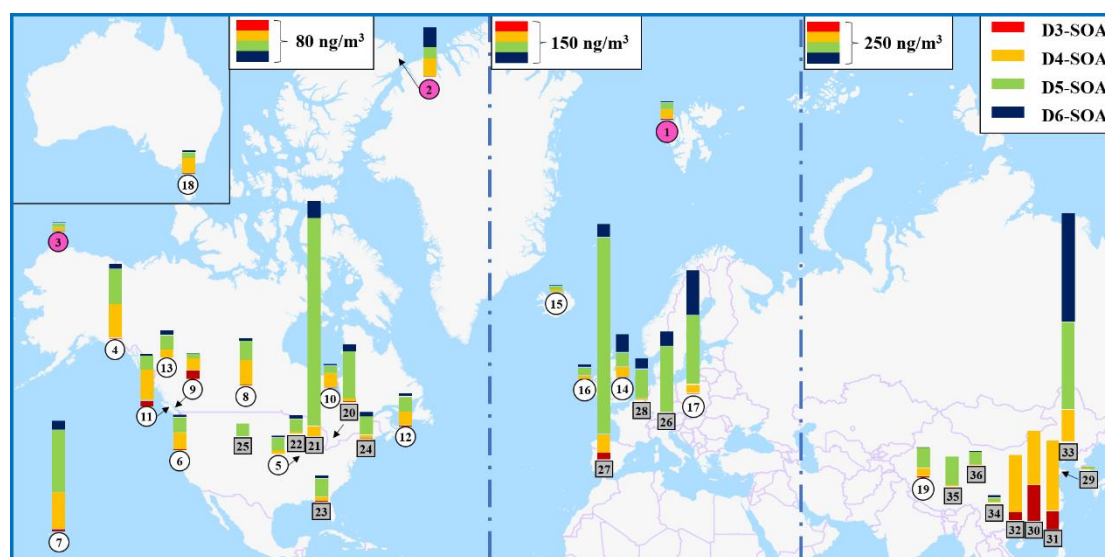
375

376   Figure 4. Global concentrations of cVMS SOA (ng/m^3) on the basis of the cVMS concentrations

377   reported from multiple studies and the cVMS SOA yields measured in this work. The numbers of polar,

378   background and urban sites are enclosed in pink, white circles and gray boxes, respectively. The details

379   about cVMS and SOA concentrations at different sites were summarized in Table S6 of the Supplement.

380

381   At urban sites in Europe and North America, cVMS SOA concentrations are reported in the range of 138-

382   813 ng/m^3 and 22.9-437 ng/m^3, respectively. Among these cVMS, D5 is the main contributor to cVMS SOA

383   at these locations, averaging 80.1% of total cVMS SOA. This contribution is higher than that (73.6%) at

384   Chinese urban sites. For instance, D5 SOA is calculated to be 684 ng/m^3 in Catalan, Spain, 387 ng/m^3 in

385   Chicago, USA, 229 ng/m^3 in Zurich, Switzerland and 99 ng/m^3 in Paris, France, where there are high levels

386   of economic activities and high population densities. These results suggest that personal care products as a

387   main source of D5 may be the most important anthropogenic origins of Si-containing SOA in Europe and

388   North America. It was noted that the D5 SOA concentration (13.38-683.57 ng/m^3) estimated here is far more

389   than that (0.016-0.206 ng/m^3) reported by Milani et al. (2021), who obtained their data using semi-quantified

390   concentrations of D$_4$TOH (first-generation D5 SOA product) extracted from PM$_{2.5}$ samples in Atlanta and

391   Houston. The difference may be mainly attributed to the missing analysis of multi-generation SOA products

392   or dimers (Wu and Johnston, 2016, 2017).   Pennington et al. (2021) utilized the developed CMAQ model

393   to investigate the concentration of D5 SOA in the urban area of Los Angeles, and the model data (21 ng/m^3)

394   was within these values here.

395   At background and Arctic sites, cVMS SOA are primarily derived from D4 and D5. The background sites

396   are located in mountains, rural areas, forested areas, lakes and at high altitudes. The three highest cVMS

397   SOA concentrations at background sites are located at Kosetice in the Czech Republic (428 ng/m^3), Hilo,

398   Hawaii, USA (203 ng/m^3) and Tibetan Plateau in China (174 ng/m^3), where the contribution percentages of

399   SOA from both D4 and D5 are 62.6%, 90.3% and 93.4%, respectively. The cVMS SOA concentrations at

400   the Little Fox Lake site in Yukon, Canada is the highest (138.8 ng/m^3) among the four locations in the Arctic,

401   91% of which is accounted for by both D4 and D5 SOA. The dominance of D4 and D5 SOA in both

402   background and the Arctic regions highlights their persistence in atmosphere and the potential for long-range

403   atmospheric transport.

404   Furthermore, global concentration distribution of Si-containing SOA estimated for the four cVMS (D3-

405   D6) at 36 sites worldwide is also presented in Table S6, which clearly shows the global importance of Si in

406   SOA with the estimated percentages of cVMS SOA that contains the Si element. For example, up to 49.2%

407   and 31.2% of cVMS SOA contained Si elements in background and urban sites, respectively. These results

408   are similar to the summary observations that reported percentages of aerosols with a Si mole fraction >0.01

409 (%) at different sites (Bzdek et al., 2014). The above results demonstrated that Si is a frequent component of

410 SOA in background and urban areas.

411   The global annual production of D4, D5 and D6 is about 1, 0.1 and 0.01 Tg·yr^{-1}, respectively, and 90% of

412 these cVMS is eventually released into the atmosphere (Li et al., 2020; Genualdi et al., 2011; Wang et al.,

413 2013; Sakurai et al., 2019). Based on the results shown in Fig. 4, the annual production of cVMS (D4-D6)

414 SOA was estimated to be 0.16 Tg·yr^{-1}, which was about 5.5% of SOA (2.9 Tg·yr^{-1}) produced from mobile

415 source emissions in the USA and 5-8 times of SOA generated by Athabasca oil sands (0.02-0.03 Tg·yr^{-1}, one

416 of the largest sources of anthropogenic secondary organic aerosols in North America) (Tkacik et al., 2014;

417 Liggio et al., 2016). Moreover, it was also 0.8% and 2.3% of isoprene-SOA (20 Tg·yr^{-1}) and monoterpenes-

418 SOA (7 Tg·yr^{-1}) (typical biogenic SOA), respectively, indicating the potential importance of cVMS SOA

419 (Jokinen et al., 2015). While these cVMS SOA sources may seem small, they can make substantially higher

420 contributions to ambient air SOAs in population centers where cVMS compounds are primarily used.

421

422 **Author contributions**

423   CH designed and conducted all experiments; CH and HY analyzed the data and prepared the paper with

424 contributions from KL, PL, JL, AL and SML. SML supervised the project.

425

426 **Competing interests**

427 The authors declare that they have no conflict of interest.

428 **Acknowledgements**

432

433   **References**

434   Ahrens, L., Harner, T., and Shoeib, M.: Temporal Variations of Cyclic and Linear Volatile Methylsiloxanes in the

435   Atmosphere Using Passive Samplers and High-Volume Air Samplers, Environ. Sci. Technol., 48, 9374-9381,

436   https://doi.org/10.1021/es502081j, 2014.

437   Allen, R., Kochs, P., and Chandra, G.: Industrial Organosilicon Materials, Their Environmental Entry and

438   Predicted Fate, Springer, 3, 1-25, https://doi.org/10.1007/978-3-540-68331-5_1, 1997.

439   Alton, M. and Browne, E.: Atmospheric Chemistry of Volatile Methyl Siloxanes: Kinetics and Products of

440   Oxidation   by   OH   Radicals   and   Cl   Atoms,   Environ.   Sci.   Technol.,   54,   5992-5999,

441   https://dx.doi.org/10.1021/acs.est.0c01368, 2020.

442   Atkinson, R.: Kinetics of the Gas-Phase Reactions of a Series of Organosilicon Compounds with OH and NO_3

443   Radicals and O_3 at 297 ± 2 K, Environ. Sci. Technol., 25, 863-866, https://doi.org/10.1021/es00017a005, 1991.

444   Bein, K., Zhao, Y., Wexler, A., Johnston, M.: Speciation of Size-Resolved Individual Ultrafine Particles in

445   Pittsburgh, Pennsylvania, J. Geophys. Res., 110, D07S05, https://doi.org/10.1029/2004jd004708, 2005.

446   Berndt, T., Richters, S., Jokinen, T., Hyttinen, N., Kurtén, T., Otkjaer, R., Kjaergaard, H., Stratmann, F., Herrmann,

447   H., Sipilä, M., Kulmala, M., and Ehn, M.: Hydroxyl Radical-Induced Formation of Highly Oxidized Organic

448   Compounds, Nat. Commun., 7, 1-8, https://doi.org/10.1038/ncomms13677, 2016.

449   Bruns, E., Haddad, I., Keller, A., Klein, F., Kumar, N., Pieber, S., Corbin, J., Slowik, J., Brune, W., Baltensperger,

450   U., and Prévôt, A.: Inter-Comparison of Laboratory Smog Chamber and Flow Reactor Systems on Organic

451   Aerosol Yield and Composition, Atmos. Meas. Tech., 8, 2315-2332, https://doi.org/10.5194/amt-8-2315-2015,

452   2015.

453   Bzdek, B., Horan, A., Pennington, M., Janechek, N., Baek, J., Stanier, C., and Johnston, M.: Silicon is a Frequent

454   Component   of   Atmospheric   Nanoparticles,   Environ.   Sci.   Technol.,   48,   11137-11145,

455   https://doi.org/10.1021/es5026933, 2014.

456   Canada, E. C. a. H.: https://www.ec.gc.ca/ese-ees/FC0D11E7-DB34-41AA-B1B3-E66EFD8813F1/batch2_540-

457   97-6_en.pdf last access: 9 February 2022, 2008.

458   Chan, A., Kautzman, K., Chhabra, P., Surratt, J., Chan, M., Crounse, J., Kürten, A., Wennberg, P., Flagan, R., and

459   Seinfeld, J.: Secondary Organic Aerosol Formation from Photooxidation of Naphthalene and Alkylnaphthalenes:

460   Implications for Oxidation of Intermediate Volatility Organic Compounds (IVOCs), Atmos. Chem. Phys., 9,

461   3049–3060, https://doi.org/10.5194/acp-9-3049-2009, 2009.

462   Chandramouli, B., Kamens, R.: The Photochemical Formation and Gas-Particle Partitioning of Oxidation

463   Products of Decamethyl Cyclopentasiloxane and Decamethyl Tetrasiloxane in the Atmosphere, Atmos.

464   Environ., 35, 87-95, https://doi.org/10.1016/S1352-2310(00)00289-2, 2001.

465   Charan, S., Huang, Y., Buenconsejo, R., Li, Q., Cocker Iii, D., and Seinfeld, J.: Secondary Organic Aerosol

466   Formation from the Oxidation of Decamethylcyclopentasiloxane at Atmospherically Relevant OH

467   Concentrations, Atmos. Chem. Phys., 22, 917-928, https://doi.org/10.5194/acp-22-917-2022, 2022.

468   Coggon, M., McDonald, B., Vlasenko, A., Veres, P., Bernard, F., Koss, A., Yuan, B., Gilman, J., Peischl, J., Aikin,

469   K., DuRant, J., Warneke, C., Li, S.-M., and Gouw, J.: Diurnal Variability and Emission Pattern of

470   Decamethylcyclopentasiloxane (D5) from the Application of Personal Care Products in Two North American

471   Cities, Environ. Sci. Technol., 52, 5610-5618, https://doi.org/10.1021/acs.est.8b00506, 2018.

472   EUR-Lex: https://eur-lex.europa.eu/legal-

473   content/EN/TXT/?uri=uriserv:OJ.L_.2018.006.01.0045.01.ENG&toc=OJ:L:2018:006:TOCECHA,   last

474   access: 25 November 2021, 2018.

475   Farasani, A. and Darbre, P.: Exposure to Cyclic Volatile Methylsiloxanes (cVMS) Causes Anchorage-Independent

476   Growth and Reduction of BRCA1 in Non-Transformed Human Breast Epithelial Cells, J. Appl. Toxicol., 37,

477   454-461, https://doi.org/10.1002/jat.3378, 2017.

478   Genualdi, S., Harner, T., Cheng, Y., Macleod, M., Hansen, K., Egmond, R., Shoeib, M., and Lee, S.: Global

479   Distribution of Linear and Cyclic Volatile Methyl Siloxanes in Air, Environ. Sci. Technol., 45, 3349-3354,

480   https://doi.org/10.1021/es200301j, 2011.

481   Glasius, M. and Goldstein, A.: Recent Discoveries and Future Challenges in Atmospheric Organic Chemistry,

482   Environ. Sci. Technol., 50, 2754-2764, https://doi.org/10.1021/acs.est.5b05105, 2016.

483   Guo, J., Zhou, Y., Cui, J., Zhang, B., and Zhang, J.: Assessment of Volatile Methylsiloxanes in Environmental

484   Matrices   and   Human   Plasma,   Sci.   Total.   Environ.,   668,   1175-1182,

485   https://doi.org/10.1016/j.scitotenv.2019.03.092, 2019.

486   Huang, Y., Coggon, M., Zhao, R., Lignell, H., Bauer, M., Flagan, R., and Seinfeld, J.: The Caltech Photooxidation

487   Flow Tube reactor: Design, Fluid Dynamics and Characterization, Atmos. Meas. Tech., 10, 839-867,

488   https://doi.org/10.5194/amt-10-839-2017, 2017.

489   Janechek, N., Hansen, K., and Stanier, C.: Comprehensive Atmospheric Modeling of Reactive Cyclic Siloxanes

and their Oxidation Products, Atmos. Chem. Phys., 17, 8357-8370, https://doi.org/10.5194/acp-17-8357-2017, 2017.

Janechek, N., Marek, R., Bryngelson, N., Singh, A., Bullard, R., Brune, W., and Stanier, C.: Physical Properties of Secondary Photochemical Aerosol from OH Oxidation of a Cyclic Siloxane, Atmos. Chem. Phys., 19, 1649-1664, https://doi.org/10.5194/acp-19-1649-2019, 2019.

Jokinen, T., Berndt, T., Makkonen, R., Kerminen, V., Junninen, H., Paasonen, P., Stratmann, F., Herrmann, H., Guenther, A., Worsnop, D., Kulmala, M., Ehn, M., and Sipilä, M.: Production of Extremely Low Volatile Organic Compounds from Biogenic Emissions: Measured Yields and Atmospheric Implications, Proc. Natl. Acad. Sci. U S A., 112, 7123-7128, https://doi.org/10.1073/pnas.1423977112, 2015.

Kierkegaard, A. and McLachlan, M.: Determination of Linear and Cyclic Volatile Methylsiloxanes in Air at a Regional Background Site in Sweden, Atmos. Environ., 80, 322-329, https://doi.org/10.1016/j.atmosenv.2013.08.001, 2013.

Kim, J. and Xu, S.: Quantitative Structure-Reactivity Relationships of Hydroxyl Radical Rate Constants for Linear and Cyclic Volatile Methylsiloxanes, Environ. Toxicol. Chem., 36, 3240-3245, https://doi.org/10.1002/etc.3914, 2017.

Kim, J., Mackay, D., and Whelan, M.: Predicted Persistence and Response Times of Linear and Cyclic Volatile Methylsiloxanes in Global and Local Environments, Chemosphere, 195, 325-335, https://doi.org/10.1016/j.chemosphere.2017.12.071, 2018.

Krogseth, I., Zhang, X., Lei, Y., Wania, F., and Breivik, K.: Calibration and Application of a Passive Air Sampler (XAD-PAS) for Volatile Methyl Siloxanes, Environ. Sci. Technol., 47, 4463-4470, https://doi.org/10.1021/es400427h, 2013a.

Krogseth, I., Kierkegaard, A., McLachlan, M., Breivik, K., Hansen, K., and Schlabach, M.: Occurrence and Seasonality of Cyclic Volatile Methyl Siloxanes in Arctic Air, Environ. Sci. Technol., 47, 502-509, https://doi.org/10.1021/es3040208, 2013b.

Lambe, A., Chhabra, P., Onasch, T., Brune, W., Hunter, J., Kroll, J., Cummings, M., Brogan, J., Parmar, Y., Worsnop, D., Kolb, C., and Davidovits, P.: Effect of Oxidant Concentration, Exposure Time, and Seed Particles on Secondary Organic Aerosol Chemical Composition and Yield, Atmos. Chem. Phys., 15, 3063-3075, https://doi.org/10.5194/acp-15-3063-2015, 2015.

Lambe, A., Ahern, A., Williams, L., Slowik, J., Wong, J., Abbatt, J., Brune, W., Ng, N., Wright, J., Croasdale, D., Worsnop, D., Davidovits, P., and Onasch, T.: Characterization of Aerosol Photooxidation Flow Reactors:

Heterogeneous Oxidation, Secondary Organic Aerosol Formation and Cloud Condensation Nuclei Activity Measurements, Atmos. Meas. Tech., 4, 445-461, https://doi.org/10.5194/amt-4-445-2011, 2011.

Lambe, A., Massoli, P., Zhang, X., Canagaratna, M., Nowak, J., Daube, C., Yan, C., Nie, W., Onasch, T., Jayne, J., Kolb, C., Davidovits, P., Worsnop, D., and Brune, W.: Controlled Nitric Oxide Production via O(^{1}D) + N$_2$O Reactions for Use in Oxidation Flow Reactor Studies, Atmos. Meas. Tech., 10, 2283-2298, https://doi.org/10.5194/amt-10-2283-2017, 2017.

Lamkaddam, H., Gratien, A., Pangui, E., Cazaunau, M., Varrault, B., and Doussin, J.: High-NO$_x$ Photooxidation of n-Dodecane: Temperature Dependence of SOA Formation, Environ Sci Technol, 51, 192-201, https://doi.org/10.1021/acs.est.6b03821, 2017.

Lee, A., Hayden, K., Herckes, P., Leaitch, W., Liggio, J., Macdonald, A., and Abbatt, J.: Characterization of Aerosol and Cloud Water at a Mountain Site During WACS 2010: Secondary Organic Aerosol Formation through Oxidative Cloud Processing, Atmos. Chem. Phys., 12, 7103-7116, https://doi.org/10.5194/acp-12-7103-2012, 2012.

Li, K., Liggio, J., Lee, P., Han, C., Liu, Q., and Li, S.-M.: Secondary Organic Aerosol Formation from α-Pinene, Alkanes, and Oil Sand-Related Precursors in a New Oxidation Flow Reactor, Atmos. Chem. Phys., 19, 9715-9731, https://doi.org/10.5194/acp-19-9715-2019, 2019a.

Li, K., Liggio, J., Han, C., Liu, Q., Moussa, S., Lee, P., and Li, S.-M.: Understanding the Impact of High-NO$_x$ Conditions on the Formation of Secondary Organic Aerosol in the Photooxidation of Oil Sand-Related Precursors, Environ. Sci. Technol., 53, 14420-14429, https://doi.org/10.1021/acs.est.9b05404, 2019b.

Li, Q., Lan, Y., Liu, Z., Wang, X., Wang, X., Hu, J., and Geng, H.: Cyclic Volatile Methylsiloxanes (cVMSs) in the Air of the Wastewater Treatment Plants in Dalian, China-Levels, Emissions, and Trends, Chemosphere, 256, 1-8, https://doi.org/10.1016/j.chemosphere.2020.127064, 2020.

Li, S.-M. and Winchester, J.: Particle Size Distribution and Chemistry of Late Winter Arctic Aerosols, J. Geophys. Res., 95, 13897-13908, https://doi.org/10.1029/J095iD09p13897, 1990.

Li, S.-M. and Winchester, J.: Aerosol Silicon and Associated Elements in the Arctic High and Mid-Troposphere, Atmos. Environ., 27, 2907-2912, https://doi.org/10.1016/0960-1686(93)90322-P, 1993.

Liggio, J., Li, S.-M., Hayden, K., Taha, Y., Stroud, C., Darlington, A., Drollette, B., Gordon, M., Lee, P., Liu, P., Leithead, A., Moussa, S., Wang, D., Brien, J., Mittermeier, R., Brook, J., Lu, G., Staebler, R., Han, Y., Tokarek, T., Osthoff, H., Makar, P., Zhang, J., Plata, D., and Gentner, D.: Oil Sands Operations as a Large Source of Secondary Organic Aerosols, Nature, 534, 91-94, https://doi.org/10.1038/nature17646, 2016.

550   Liu, N., Xu, L., and Cai, Y.: Methyl Siloxanes in Barbershops and Residence Indoor Dust and the Implication for

551   Human Exposures, Sci. Total. Environ., 618, 1324-1330, https://doi.org/10.1016/j.scitotenv.2017.09.250, 2018.

552   Mao, J., Ren, X., Brune, W., Olson, J., Crawford, J., Fried, A., Huey, L., Cohen, R., Heikes, B., Singh, H., Blake,

553   D., Sachse, G., Diskin, G., Hall, S., and Shetter, R.: Airborne Measurement of OH Reactivity during INTEX-

554   B, Atmos. Chem. Phys., 9, 163-173, https://doi.org/10.5194/acp-9-163-2009, 2009.

555   McFiggans, G., Mentel, T., Wildt, J., Pullinen, I., Kang, S., Kleist, E., Schmitt, S., Springer, M., Tillmann, R., Wu,

556   C., Zhao, D., Hallquist, M., Faxon, C., Breton, M., Hallquist, A., Simpson, D., Bergström, R., Jenkin, M., Ehn,

557   M., Thornton, J., Alfarra, M., Bannan, T., Percival, C., Priestley, M., Topping, D., and Scharr, A.: Secondary

558   Organic Aerosol Reduced by Mixture of Atmospheric Vapours, Nature, 565, 587-593,

559   https://doi.org/10.1038/s41586-018-0871-y, 2019.

560   Milani, A., Al-Naiema, I., and Stone, E.: Detection of a Secondary Organic Aerosol Tracer Derived from Personal

561   Care Products, Atmos. Environ., 246, https://doi.org/10.1016/j.atmosenv.2020.118078, 2021.

562   Ng, N., Kroll, J., Chan, A., Chhabra, P., Flagan, R., and Seinfeld, J.: Secondary Organic Aerosol Formation from

563   m-Xylene, Toluene, and Benzene, Atmos. Chem. Phys., 7, 3909–3922, https://doi.org/10.5194/acp-7-3909-

564   2007, 2007a.

565   Ng, N., Chhabra, P., Chan, A., Surratt, J., Kroll, J., Kwan, A., McCabe, D., Wennberg, P., Sorooshian, A., Murphy,

566   S., Dalleska, N., Flagan, R., and Seinfeld, J.: Effect of NO_x Level on Secondary Organic Aerosol (SOA)

567   Formation from the Photooxidation of Terpenes, Atmos. Chem. Phys., 7, 5159–5174,

568   https://doi.org/10.5194/acp-7-5159-2007, 2007b.

569   Ng, N., Canagaratna, M., Zhang, Q., Jimenez, J., Tian, J., Ulbrich, I., Kroll, J., Docherty, K., Chhabra, P., Bahreini,

570   R., Murphy, S., Seinfeld, J., Hildebrandt, L., Donahue, N., DeCarlo, P., Lanz, V., Prévôt, A., Dinar, E., Rudich,

571   Y., and Worsnop, D.: Organic Aerosol Components Observed in Northern Hemispheric Datasets from Aerosol

572   Mass Spectrometry, Atmos. Chem. Phys., 10, 4625-4641, https://doi.org/10.5194/acp-10-4625-2010, 2010.

573   Peng, Z., Taylor, J., Orlando, J., Tyndall, G., and Jimenez, J.: Organic Peroxy Radical Chemistry in Oxidation

574   Flow Reactors and Environmental Chambers and their Atmospheric Relevance, Atmos. Chem. Phys., 19, 813-

575   834, https://doi.org/10.5194/acp-19-813-2019, 2019.

576   Peng, Z., Palm, B., Day, D., Talukdar, R., Hu, W., Lambe, A., Brune, W., and Jimenez, J.: Model Evaluation of

577   New Techniques for Maintaining High-NO Conditions in Oxidation Flow Reactors for the Study of OH-

578   Initiated Atmospheric Chemistry, ACS. Earth. Space. Chem. , 2, 72-86,

579   https://doi.org/10.1021/acsearthspacechem.7b00070, 2017.

580 Pennington, E., Seltzer, K., Murphy, B., Qin, M., Seinfeld, J., and Pye, H.: Modeling Secondary Organic Aerosol

581 Formation from Volatile Chemical Products, Atmos. Chem. Phys., 21, 18247-18261,

582 https://doi.org/10.5194/acp-21-18247-2021, 2021.

583 Phares, D., Rhoads, K., Johnston, M., and Wexler, A.: Size-Resolved Ultrafine Particle Composition Analysis 2.

584 Houston, J. Geophys. Res., 108, 1-14, https://doi.org/10.1029/2001jd001212, 2003.

585 Presto, A., Hartz, K., and Donahue, N.: Secondary Organic Aerosol Production from Terpene Ozonolysis. 2. Effect

586 of NO_x Concentration, Environ. Sci. Technol. , 39, 7046-7054, https://doi.org/10.1021/es050400s, 2005.

587 Rauert, C., Shoieb, M., Schuster, J., Eng, A., and Harner, T.: Atmospheric Concentrations and Trends of Poly- and

588 Perfluoroalkyl Substances (PFAS) and Volatile Methyl Siloxanes (VMS) over 7 Years of Sampling in the Global

589 Atmospheric Passive Sampling (GAPS) Network, Environ. Pollut., 238, 94-102,

590 https://doi.org/10.1016/j.envpol.2018.03.017, 2018.

591 Rhoads, K., Phares, D., Wexler, A., Johnston, M.: Size-Resolved Ultrafine Particle Composition Analysis 1.

592 Atlanta, J. Geophys. Res., 108, 1-13, https://doi.org/10.1029/2001jd001211, 2003.

593 Riipinen, I., Juuti, T., Pierce, J., Petäjä, T., Worsnop, D., Kulmala, M., and Donahue, N.: The Contribution of

594 Organics to Atmospheric Nanoparticle Growth, Nat. Geosci., 5, 453-458, https://doi.org/10.1038/ngeo1499,

595 2012.

596 Rücker, C. and Kümmerer, K.: Environmental Chemistry of Organosiloxanes, Chem. Rev., 115, 466-524,

597 https://doi.org/10.1021/cr500319v, 2015.

598 Safron, A., Strandell, M., Kierkegaard, A., and Macleod, M.: Rate Constants and Activation Energies for Gas-

599 Phase Reactions of Three Cyclic Volatile Methyl Siloxanes with the Hydroxyl Radical, Int. J. Chem. Kinet., 47,

600 420-428, https://doi.org/10.1002/kin.20919, 2015.

601 Sakurai, T., Imaizumi, Y., Kuroda, K., Hayashi, T., and Suzuki, N.: Georeferenced multimedia environmental fate

602 of volatile methylsiloxanes modeled in the populous Tokyo Bay catchment basin, Sci Total Environ, 689, 843-

603 853, https://doi.org/10.1016/j.scitotenv.2019.06.462, 2019.

604 Sarrafzadeh, M., Wildt, J., Pullinen, I., Springer, M., Kleist, E., Tillmann, R., Schmitt, S., Wu, C., Mentel, T., Zhao,

605 D., Hastie, D., and Scharr, A.: Impact of NO_x and OH on Secondary Organic Aerosol Formation from β-Pinene

606 Photooxidation, Atmos. Chem. Phys., 16, 11237-11248, https://doi.org/10.5194/acp-16-11237-2016, 2016.

607 Simonen, P., Saukko, E., Karjalainen, P., Timonen, H., Bloss, M., Saksa, P., Rönkkö, T., Keskinen, J., and Maso,

608 M.: A New Oxidation Flow Reactor for Measuring Secondary Aerosol Formation of Rapidly Changing

609 Emission Sources, Atmos. Meas. Tech., 10, 1519-1537, https://doi.org/10.5194/amt-10-1519-2017, 2017.

610 Sommerlade, R., Parlar, H., Wrobel, D , Kochs, P.: Product Analysis and Kinetics of the Gas-Phase Reactions of

611 Selected Organosilicon Compounds with OH Radicals Using a Smog Chamber-Mass Spectrometer System,

612 Environ. Sci. Technol., 27, 2435-2440, https://doi.org/10.1021/es00048a019, 1993.

613 Tang, X., Misztal, P., Nazaroff, W., and Goldstein, A.: Siloxanes Are the Most Abundant Volatile Organic

614 Compound Emitted from Engineering Students in a Classroom, Environ. Sci. Technol. Lett. , 2, 303-307,

615 https://doi.org/10.1021/acs.estlett.5b00256, 2015.

616 Tkacik, D., Lambe, A., Jathar, S., Li, X., Presto, A., Zhao, Y., Blake, D., Meinardi, S., Jayne, J., Croteau, P., and

617 Robinson, A.: Secondary Organic Aerosol Formation from in-Use Motor Vehicle Emissions Using a Potential

618 Aerosol Mass Reactor, Environ. Sci. Technol., 48, 11235-11242, https://doi.org/10.1021/es502239v, 2014.

619 Wang, D.-G., Norwood, W., Alaee, M., Byer, J., and Brimble, S.: Review of Recent Advances in Research on the

620 Toxicity, Detection, Occurrence and Fate of Cyclic Volatile Methyl Siloxanes in the Environment, Chemosphere,

621 93, 711-725, https://doi.org/10.1016/j.chemosphere.2012.10.041, 2013.

622 Wang, X., Schuster, J., Jones, K., and Gong, P.: Occurrence and Spatial Distribution of Neutral Perfluoroalkyl

623 Substances and Cyclic Volatile Methylsiloxanes in the Atmosphere of the Tibetan Plateau, Atmos. Chem. Phys.,

624 18, 8745-8755, https://doi.org/10.5194/acp-18-8745-2018, 2018.

625 Wang, X., Lee, S., Sheng, G., Chan, L., Fu, J., Li, X., Min, Y., and Chan, C.: Cyclic organosilicon compounds in

626 ambient air in Guangzhou, Macau and Nanhai, Pearl River Delta, Appl. Geochemistry, 16, 1447-1454,

627 https://doi.org/10.1016/S0883-2927(01)00044-0, 2001.

628 Wildt, J., Mentel, T., Scharr, A., Hoffmann, T., Andres, S., Ehn, M., Kleist, E., Müsgen, P., Rohrer, F., Rudich, Y.,

629 Springer, M., Tillmann, R., and Wahner, A.: Suppression of New Particle Formation from Monoterpene

630 Oxidation by NO_x, Atmos. Chem. Phys., 14, 2789-2804, https://doi.org/10.5194/acp-14-2789-2014, 2014.

631 Wu, Y. and Johnston, M.: Molecular Characterization of Secondary Aerosol from Oxidation of Cyclic

632 Methylsiloxanes, J. Am. Soc. Mass Spectrom., 27, 402-409, https://doi.org/10.1007/s13361-015-1300-1, 2016.

633 Wu, Y. and Johnston, M.: Aerosol Formation from OH Oxidation of the Volatile Cyclic Methyl Siloxane (cVMS)

634 Decamethylcyclopentasiloxane, Environ. Sci. Technol., 51, 4445-4451,

635 https://doi.org/10.1021/acs.est.7b00655, 2017.

636 Xiao, R., Zammit, I., Wei, Z., Hu, W.-P., MacLeod, M., and Spinney, R.: Kinetics and Mechanism of the Oxidation

637 of Cyclic Methylsiloxanes by Hydroxyl Radical in the Gas Phase: An Experimental and Theoretical Study,

638 Environ. Sci. Technol., 49, 13322-13330, https://doi.org/10.1021/acs.est.5b03744, 2015.

639 Xu, S., Warner, N., Nizzetto, P., Durham, J., and McNett, D.: Long-Range Transport Potential and Atmospheric

640   Persistence of Cyclic Volatile Methylsiloxanes Based on Global Measurements, Chemosphere, 228, 460-468,

641   https://doi.org/10.1016/j.chemosphere.2019.04.130, 2019.

642   Zhao, D., Schmitt, S., Wang, M., Acir, I., Tillmann, R., Tan, Z., Novelli, A., Fuchs, H., Pullinen, I., Wegener, R.,

643   Rohrer, F., Wildt, J., Scharr, A., Wahner, A., and Mentel, T.: Effects of NO_x and SO_2 on the Secondary Organic

644   Aerosol Formation from Photooxidation of α-Pinene and Limonene, Atmos. Chem. Phys., 18, 1611-1628,

645   https://doi.org/10.5194/acp-18-1611-2018, 2018.

646   Zhou, C., Jang, M., and Yu, Z.: Simulation of SOA Formation from the Photooxidation of Monoalkylbenzenes in

647   the Presence of Aqueous Aerosols Containing Electrolytes under Various NO_x Levels, Atmos. Chem. Phys., 19,

648   5719-5735, https://doi.org/10.5194/acp-19-5719-2019, 2019.

649